

# The Importance of Hemorheology and Patient Anatomy on the Hemodynamics in the Inferior Vena Cava

KENNETH I. AYCOCK,<sup>1,2</sup> ROBERT L. CAMPBELL,<sup>1,3</sup> FRANK C. LYNCH,<sup>4</sup> KEEFE B. MANNING,<sup>2,4</sup> and BRENT A. CRAVEN<sup>5</sup>

<sup>1</sup>Applied Research Laboratory, The Pennsylvania State University, University Park, PA, USA; <sup>2</sup>Department of Biomedical Engineering, The Pennsylvania State University, University Park, PA, USA; <sup>3</sup>Department of Mechanical and Nuclear Engineering, The Pennsylvania State University, University Park, PA, USA; <sup>4</sup>Department of Surgery, Penn State Hershey Medical Center, Hershey, PA, USA; and <sup>5</sup>Division of Applied Mechanics, Office of Science and Engineering Laboratories, Center for Devices and Radiological Health, U.S. Food and Drug Administration, Silver Spring, MD, USA

(Received 23 February 2016; accepted 27 May 2016; published online 6 June 2016)

Associate Editor Andreas Anayiotos oversaw the review of this article.

**Abstract**—Inferior vena cava (IVC) filters have been used for nearly half a century to prevent pulmonary embolism in at-risk patients. However, complications with IVC filters remain common. In this study, we investigate the importance of considering the hemorheological and morphological effects on IVC hemodynamics by simulating Newtonian and non-Newtonian blood flow in three IVC models with varying levels of geometric idealization. Partial occlusion by an IVC filter and a thrombus is also considered. More than 99% of the infrarenal IVC volume is found to contain flow in the nonlinear region of the shear rate–viscosity curve for blood (less than  $100 \text{ s}^{-1}$ ) in the unoccluded IVCs. Newtonian simulations performed using the asymptotic viscosity for blood over-predict the non-Newtonian Reynolds numbers by more than a factor of two and under-predict the mean wall shear stress (WSS) by 28–54%. Agreement with the non-Newtonian simulations is better using a characteristic viscosity, but local WSS errors are still large (up to 50%) in the partially occluded cases. Secondary flow patterns in the IVC also depend on the viscosity model and IVC morphological complexity. Non-Newtonian simulations required only a marginal increase in computational expense compared with the Newtonian simulations. We recommend that future studies of IVC hemodynamics consider the effects of hemorheology and IVC morphology when accurate predictions of WSS and secondary flow features are desired.

**Keywords**—Non-Newtonian blood flow, Patient-specific modeling, Shear-rate histograms, Computational fluid dynamics, Wall shear stress, Blood viscosity, IVC filter.

## INTRODUCTION

Pulmonary embolism (PE) is a life-threatening condition that occurs when an embolus travels into the pulmonary arteries and occludes blood flow to the lungs. Although PE is normally prevented using anticoagulation therapy, when anticoagulants are contraindicated, an inferior vena cava (IVC) filter may instead be placed to act as a mechanical barrier to embolus passage.

Most IVC filters are composed of a series of round or rectangular metal struts arranged in a conical shape and connected at a central hub (e.g., Greenfield (Boston Scientific Corporation, Natick, MA); Günther Tulip and Celect (Cook Medical, Bloomington, IN); Option (Angiotech, Vancouver, BC, Canada); ALN (ALN Implants Chirurgicaux, Ghisonaccia, France); and G2 Express, Eclipse, Meridian, Denali, and Simon Nitinol filters (Bard Peripheral Vascular, Tempe, AZ)). The filter struts direct emboli toward the filter hub at the center of the IVC lumen where the emboli are captured and, ideally, slowly undergo lysis under the influence of fluid shear stresses.<sup>43,45</sup> However, the presence of the IVC filter may also disrupt IVC hemodynamics, causing secondary flow downstream of the filter struts and hub that can promote thrombosis.<sup>39,40,43,45,50</sup>

The number of filters placed in the United States annually has increased rapidly over the past few years, from 2000 in 1979<sup>4</sup> to 132,000 in 2007,<sup>28</sup> to an estimated 250,000 in 2012.<sup>41</sup> Despite decades of clinical use and development, complications with modern IVC filters remain common<sup>13</sup> and include recurrence of PE,

---

Address correspondence to Keefe B. Manning, Department of Biomedical Engineering, The Pennsylvania State University, University Park, PA, USA. Electronic mail: kbm10@psu.edu

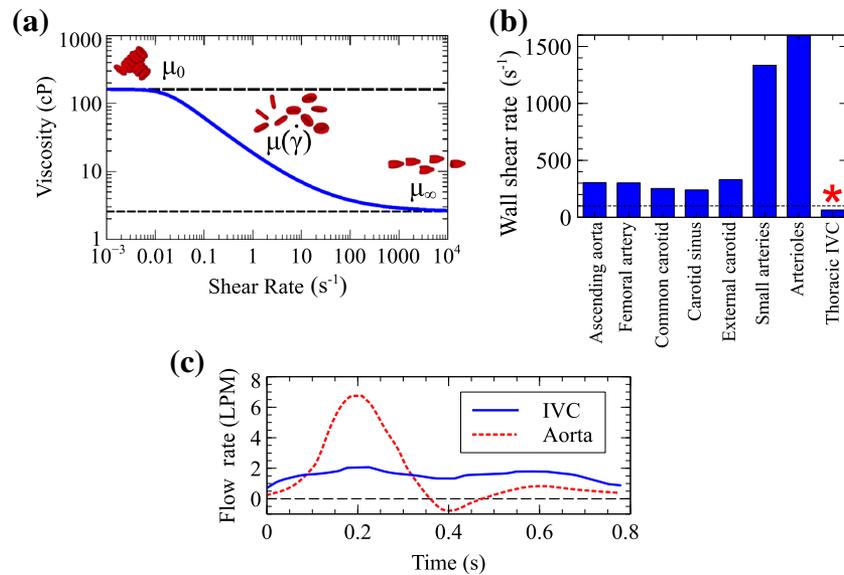


**FIGURE 1.** (a) Shear rate–viscosity curve for blood with RBC disaggregation and deformation illustrated. (b) Mean wall shear rate (WSR) in various vessels of the human circulation (data from Goldsmith and Turitto<sup>22</sup>). The dashed line indicates a WSR of 100 s<sup>-1</sup>. (c) Flow waveforms for the human descending aorta and infrarenal IVC under resting conditions based on *in vivo* magnetic resonance imaging measurements.<sup>9</sup> The data show that flow through the IVC is approximately steady.

persistence or worsening of deep-vein thrombosis, filter fracture, filter perforation, and filter migration. Furthermore, although previous studies<sup>23,50</sup> have outlined the attributes of an “ideal” IVC filter (e.g., non-thrombogenic, high embolus-trapping efficiency, and resistance to tilt or migration), a single “ideal” IVC filter may not exist for all patients, as the best combination of filter characteristics is likely patient-specific.<sup>43</sup>

Computational modeling has the ability to predict the local mechanical and hemodynamic parameters that determine the *in vivo* performance of IVC filters and could, with further development and validation, be used as a tool to guide clinical decisions (e.g., filter selection and filter placement location) on a patient-specific basis. To date, previous studies used finite element analysis to predict vein-IVC filter contact forces,<sup>1,16</sup> the force required for an IVC filter to migrate downstream,<sup>19</sup> and the force required for penetration of an IVC filter strut through the IVC wall.<sup>24</sup> Researchers have also used computational fluid dynamics (CFD) to predict the effect of IVC filter placement on secondary flow patterns and wall shear stresses (WSS) in the IVC.<sup>1,38,39,43,50</sup>

In these computational studies, two primary simplifications are made. First, the geometry of the human IVC is idealized, either as a single straight tube,<sup>39,43,45</sup> or as a smooth tube with straight side branches.<sup>38,50</sup> In reality, the IVC and its branches pass through the abdomen in close proximity to the aorta, the lumbar

spine, and the various organs of the gastrointestinal system. Consequently, the morphology of the IVC is complex: the cross section of the IVC is non-circular and varies in shape and size along the length of the vessel, the IVC and its branches are curved, and anatomical variants such as asymptomatic iliac vein compression are common.<sup>36</sup>

Second, in previous studies blood is approximated as a Newtonian fluid,<sup>1,38,39,43,50</sup> neglecting its shear-thinning and viscoelastic properties. High shear rates disrupt red blood cell (RBC) aggregates and deform RBCs into shapes that reduce drag.<sup>11</sup> Thus, the effective viscosity of blood decreases with increasing shear rate until reaching an asymptotic value for shear rates above approximately 100 s<sup>-1</sup> (Fig. 1a). In most computational hemodynamic studies, shear rates are assumed to be sufficiently high to justify the approximation of blood as a Newtonian fluid with a viscosity equal to its asymptotic value. Shear rates in the IVC, however, are among the lowest in the circulation (Fig. 1b), in part due to the lack of flow pulsatility (Fig. 1c). Furthermore, a recent study<sup>10</sup> shows that secondary flows patterns are sensitive to hemorheology in large, curved blood vessels like the IVC.

In this study, we investigate hemorheological and morphological effects on IVC hemodynamics. Specifically, we compare velocity profiles, secondary flows, IVC and thrombus WSS, and thrombus wake volumes among three IVC geometries with varying levels of idealization. Newtonian and non-Newtonian blood

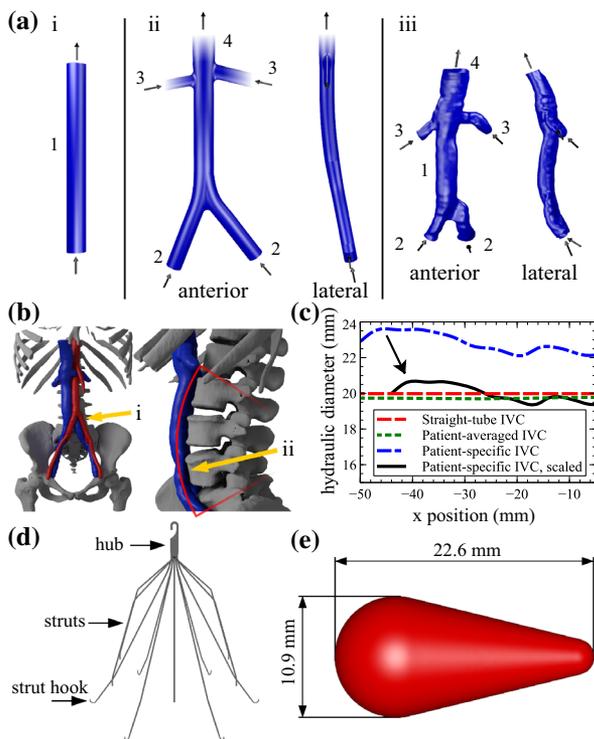


**FIGURE 2.** (a) Anterior and lateral views of the three-dimensional models for the (i) straight tube IVC, (ii) patient-averaged IVC, and (iii) patient-specific IVC, with the following vessel segments: 1—infrarenal IVC, 2—iliac veins, 3—renal veins, and 4—suprarenal IVC. Geometries are shown in order of increasing geometric complexity from left to right. (b) Anatomical details captured in the patient-specific IVC geometry: (i) compression of the left iliac vein between the right iliac artery (anterior) and the spine (posterior); (ii) curvature of the infrarenal IVC along the lumbar spine. (c) Hydraulic diameters for the infrarenal regions of the IVCs. The average hydraulic diameter for the straight tube, patient-averaged, and scaled patient-specific IVCs is approximately 2 cm. The location  $x = 0$  mm is approximately 2 cm upstream of where the renal veins meet the IVC in the patient-averaged and patient-specific IVCs. (d) Computational model of the G2 Express IVC filter and (e) teardrop-shaped thrombus.

flow simulations are performed, and non-Newtonian effects are quantified by calculating non-Newtonian importance factors and the local and mean errors in velocities, shear rates, and shear stresses due to the Newtonian approximation. Accurately predicting these quantities (in particular, WSS) is important for modeling and simulation of thrombosis, thrombolysis, embolization, and embolus migration.

## MATERIALS AND METHODS

### Computational Geometries

Three IVC geometries are considered (Fig. 2a): (1) a straight, circular tube IVC, (2) a patient-averaged IVC based on measurements from ten computed

**TABLE 1.** Maximum (max.), minimum (min.), and average (avg.) contact normal force magnitudes for the three IVC geometries.

Force (mN)	IVC geometry		
	Straight-tube	Patient-averaged	Scaled patient-specific
Max.	14	22	26
Min.	9.6	5.5	7.2
Avg.	12	12	13
%SD	19	41	45

The percent standard deviation (%SD) of the contact normal force magnitude is also shown.

tomography (CT) datasets,<sup>38</sup> and (3) a patient-specific IVC representative of a normal patient with a healthy level of left common iliac vein compression by the right iliac artery (approximately 41% compression here vs. an observed range for asymptomatic compression of 0–68%;<sup>36</sup> Fig. 2b). The CT data for the patient-specific IVC was acquired (in-plane resolution of 0.59 mm and slice offset of 0.7 mm) at the Hershey Medical Center after obtaining an IRB exemption. As in Aycock *et al.*,<sup>1</sup> the CT data were then segmented and reconstructed to produce a three-dimensional model of the patient IVC. The patient-specific IVC was uniformly scaled by a factor of 0.88 to obtain a mean hydraulic diameter of 2 cm, approximately the same as that of the patient-averaged and straight-tube IVCs (Fig. 2c). This was required to achieve both dynamic similarity and comparable mean shear rates in each IVC geometry, thereby enabling consistent comparisons when examining the influence of non-Newtonian effects.

Partial occlusion of the IVCs by an IVC filter (G2 Express, Bard Peripheral Vascular, Tempe, AZ; Fig. 2d) and a teardrop-shaped<sup>15,38,43</sup> thrombus (approximately 1.06 cm<sup>3</sup> in volume; maximum occlusion of approximately 30% of the cross-sectional area of the infrarenal IVC; Fig. 2e) was considered using a nonlinear finite element-based computational method for virtual filter placement from a previous study.<sup>1</sup> In brief, an inverse analysis was performed to approximate the *in vivo* stress state of each IVC. The sheathed IVC filter was then positioned in the infrarenal region of each IVC and virtually placed by simulating contact between the vein wall and the IVC filter. The IVC was modeled as a compliant anisotropic, hyperelastic vessel<sup>1,20</sup> during the filter placement simulation, but was modeled as a rigid structure in the hemodynamics simulations. The virtual placement simulations reveal that the normal contact forces between the vein wall and the IVC filter struts are increasingly non-uniform with increasing geometric complexity (Table 1), in agreement with a recent study on IVC filter forces.<sup>16</sup>

### Characteristic Shear Rate and Viscosity

In previous literature,<sup>2,8,21,30</sup> a characteristic viscosity has been used to improve the accuracy of the Newtonian approximation. Phenomenologically, use of a characteristic viscosity scales the Reynolds number of the Newtonian flow so that it approximately matches the Reynolds number of the non-Newtonian flow.<sup>21</sup> The characteristic viscosity may be calculated based on either the wall shear rate (WSR),<sup>12,31</sup> which is usually the highest shear rate in the flow, or based on the mean shear rate.<sup>2,3,8,21,46</sup>

For simple Poiseuille flow of a Newtonian fluid in a vessel of circular cross section, the mean shear rate<sup>30,46</sup> is:

$$\dot{\gamma}_p = \frac{16U}{3D} \quad (1)$$

where  $U$  is the characteristic velocity and  $D$  is the vessel diameter. However, because the patient-averaged and patient-specific IVC geometries considered in the current study are more complex, with curved vessels and bifurcations, the flow deviates significantly from Poiseuille flow. Therefore, we used a more rigorous procedure for estimating the characteristic shear rate and viscosity:

- (1) Perform a Newtonian simulation using an asymptotic viscosity  $\mu_\infty$  for blood.
- (2) Calculate a characteristic shear rate  $\dot{\gamma}_c$  for the flow based on a representative mean shear rate. For example, for a cell-centered finite volume method, a volume-weighted shear rate may be calculated as:

$$\dot{\gamma}_c = \frac{\sum_{i=1}^n \dot{\gamma}_i V_i}{\sum_{i=1}^n V_i} \quad (2)$$

where  $\dot{\gamma}_i$  are the cell-centered shear rate values and  $V_i$  are the cell volumes.

- (3) Use the characteristic shear rate  $\dot{\gamma}_c$  to calculate a corresponding characteristic viscosity with the chosen non-Newtonian viscosity model, i.e.  $\mu_c = \mu(\dot{\gamma}_c)$ .
- (4) Perform a second Newtonian simulation using the obtained characteristic viscosity  $\mu_c$ .

Following this procedure, a Newtonian simulation was first performed in each of the IVCs using the asymptotic viscosity. Characteristic shear rates were calculated based on the volume-weighted mean shear rate in the infrarenal regions of the IVCs, where IVC filters are generally placed. A second Newtonian simulation was then performed in each IVC using the resulting characteristic viscosity. This process was repeated for the partially occluded IVCs.

### Non-Newtonian Model and Non-Newtonian Reynolds Number

Non-Newtonian simulations were performed in each IVC using the Carreau model.<sup>6</sup> Unlike other models (e.g., power-law), the Carreau model captures the asymptotic behavior of shear-thinning fluids at both low and high shear rates, making it a popular choice for modeling blood flow.<sup>8,21,32,45,48</sup> The Carreau model assumes that the viscosity is a function of the local shear rate:

$$\mu(\dot{\gamma}) = \mu_\infty + (\mu_0 - \mu_\infty) \left(1 + (\lambda\dot{\gamma})^2\right)^{\frac{n-1}{2}} \quad (3)$$

where  $\mu_\infty$  is the asymptotic viscosity,  $\mu_0$  is the zero shear rate viscosity,  $\lambda$  is the relaxation time for blood,  $\dot{\gamma}$  is the scalar shear rate, and  $n$  determines the transition between the low and high viscosities. The scalar shear rate ( $\dot{\gamma}$ ) may be defined in tensor notation as:<sup>6</sup>

$$\dot{\gamma} = \sqrt{2e_{ij}e_{ij}} \quad (4)$$

where  $e_{ij}$  is the strain rate tensor:<sup>27</sup>

$$e_{ij} = \frac{1}{2} \left( \frac{\partial u_i}{\partial x_j} + \frac{\partial u_j}{\partial x_i} \right).$$

Constants used for the Carreau model were the same as those used in a previous study<sup>45</sup> of non-Newtonian blood flow in a simplified IVC ( $\mu_\infty = 2.57$  cP,  $\mu_0 = 162.66$  cP,  $\lambda = 57.49$  s, and  $n = 0.435$ ).

For the non-Newtonian simulations, the Reynolds number ( $Re$ ) was calculated as:<sup>2,3,21,30</sup>

$$Re = \frac{\rho UD}{\mu_{c,n-N}} \quad (6)$$

where  $\rho$  is the fluid density,  $U$  is the characteristic velocity,  $D$  is the characteristic diameter, and  $\mu_{c,n-N}$  is the characteristic viscosity calculated from the Carreau model using the volume-weighted mean shear rate (Eq. 2) from the non-Newtonian flow. Because the cross sections of the infrarenal IVCs are not perfectly circular, the hydraulic diameter (calculated as  $D_h = 4A/P$ , where  $A$  is the cross-sectional area and  $P$  the wetted perimeter) was used as the characteristic diameter in the Reynolds number (Eq. 6).

### Quantifying Non-Newtonian Effects

To quantify the non-Newtonian effects and the error incurred by the Newtonian approximation, percent standard deviation (%SD) and percent mean error (%ME) were calculated as:

$$\%SD(\phi) = \frac{1}{\bar{\phi}_{n-N}} \sqrt{\frac{\sum_{i=1}^n (\bar{\phi}_{n-N} - \phi_{n-N,i})^2 A_i}{\sum_{i=1}^n A_i}} \times 100 \quad (7)$$

$$\%ME(\phi) = \frac{1}{\bar{\phi}_{n-N}} \frac{\sum_{i=1}^n (\phi_N - \phi_{n-N,i}) A_i}{\sum_{i=1}^n A_i} \times 100 \quad (8)$$

respectively, where  $\phi$  is either the wall viscosity ( $\mu_{\text{wall}}$ ), WSR, or WSS,  $\phi_N$  is the corresponding value obtained using the Newtonian approximation,  $\phi_{n-N}$  is the corresponding value obtained from the non-Newtonian simulations,  $A_i$  are the areas for face-area weighting (e.g., see Fortuny *et al.*<sup>17</sup>), and  $i$  sums over all faces in the infrarenal region of each IVC. Mean values of  $\phi$  were also calculated using face-area weighting:

$$\bar{\phi} = \frac{\sum_{i=1}^n \phi_i A_i}{\sum_{i=1}^n A_i} \quad (9)$$

The %SD quantifies the variability of the non-Newtonian values and, thereby, the importance of non-Newtonian effects (i.e., the larger the spread in WSR and  $\mu_{\text{wall}}$ , the greater the importance of considering hemorheological effects), while the %ME quantifies the bias in the Newtonian approximation (i.e., whether the Newtonian approximation under-predicts or over-predicts values, on average). Mean error values normalized by the field means are reported rather than the average of percent error values calculated on a per cell basis due to the occurrence of some values of  $\phi$  close to zero (e.g., in stagnation regions), which would result in percent error values approaching positive or negative infinity. That is, we normalize the mean errors by the mean field values to accommodate zero-valued regions that would otherwise be problematic.

The importance of non-Newtonian effects was also characterized using the non-Newtonian importance factor proposed by Ballyk *et al.*,<sup>3</sup> which is the ratio of the characteristic viscosity to the asymptotic viscosity ( $\mu_c/\mu_\infty$ ). According to Ballyk *et al.*,<sup>3</sup> for values of  $\mu_c/\mu_\infty > 1.75$ , non-Newtonian effects are significant.

### Quantifying Geometric Effects

The geometric tortuosity of the each infrarenal IVC was quantified using the non-dimensional tortuosity index<sup>7</sup> ( $\tau$ ):

$$\tau = \frac{L}{L_0} \quad (10)$$

where  $L_0$  is the shortest distance between two points lying at the ends of a section of a vessel and  $L$  is the distance between the two endpoints following the centerline of the vessel lumen. Tortuosity was calcu-

lated for the infrarenal region of each IVC by extracting the infrarenal centerlines in Avizo (VSG Inc., Burlington, MA, USA) using the skeletalization tool. The tortuosity indices are 1, 1.01, and 1.05 for the straight-tube, patient-averaged, and scaled patient-specific IVCs, respectively.

The Dean number ( $De$ ) was also calculated for the infrarenal regions of the IVCs to quantify the effect of infrarenal curvature on IVC hemodynamics. The Dean number is a dimensionless parameter that characterizes the strength of counter-rotating vortices (i.e., Dean flow) in curved pipes and is a function of geometry and Reynolds number:

$$De = Re \left( \frac{D}{2R} \right)^{1/2} \quad (11)$$

where  $D$  is the (hydraulic) diameter of the pipe and  $R$  is the radius of curvature of the pipe along the flow direction. The presence of Dean vortices in the IVCs was confirmed by visualizing velocity vectors and contours on slices perpendicular to the direction of the bulk flow.

The influence of geometric complexity on IVC hemodynamics was also evaluated by comparing shear rate histograms, velocity, shear rate, and shear stress profiles, non-Newtonian importance factors, and Newtonian approximation errors among the three IVCs.

### Numerical Methods

Blood flow was simulated using the finite volume method to solve the laminar, incompressible Navier-Stokes equations in OpenFOAM (version 2.3.x, OpenCFD, Ltd). Hexahedral-dominant volume meshes of the IVCs were created before and after filter and thrombus placement. Meshes were generated with the same spatial resolution as the patient-specific IVC meshes in a previous study,<sup>1</sup> yielding meshes containing approximately 8 million to 13 million computational cells. Wall normal layers were added on the surfaces of the IVC, the filter, and the thrombus to improve the accuracy of near-wall velocity gradient calculations. A mesh refinement study was performed previously in a patient-specific IVC at a higher Reynolds number than considered in the current study, which yielded a grid convergence index of approximately 6%.<sup>1</sup>

Simulations were performed in each IVC considering three occlusion scenarios (unoccluded, partially occluded by an IVC filter, and partially occluded by an IVC filter and thrombus) and three different viscosity models (27 CFD simulations, total). Newtonian simulations were performed using asymptotic and characteristic viscosities ( $\mu_\infty$  and  $\mu_c$ ), and non-Newtonian simulations were performed using the Carreau model. Blood was modeled with a constant density of

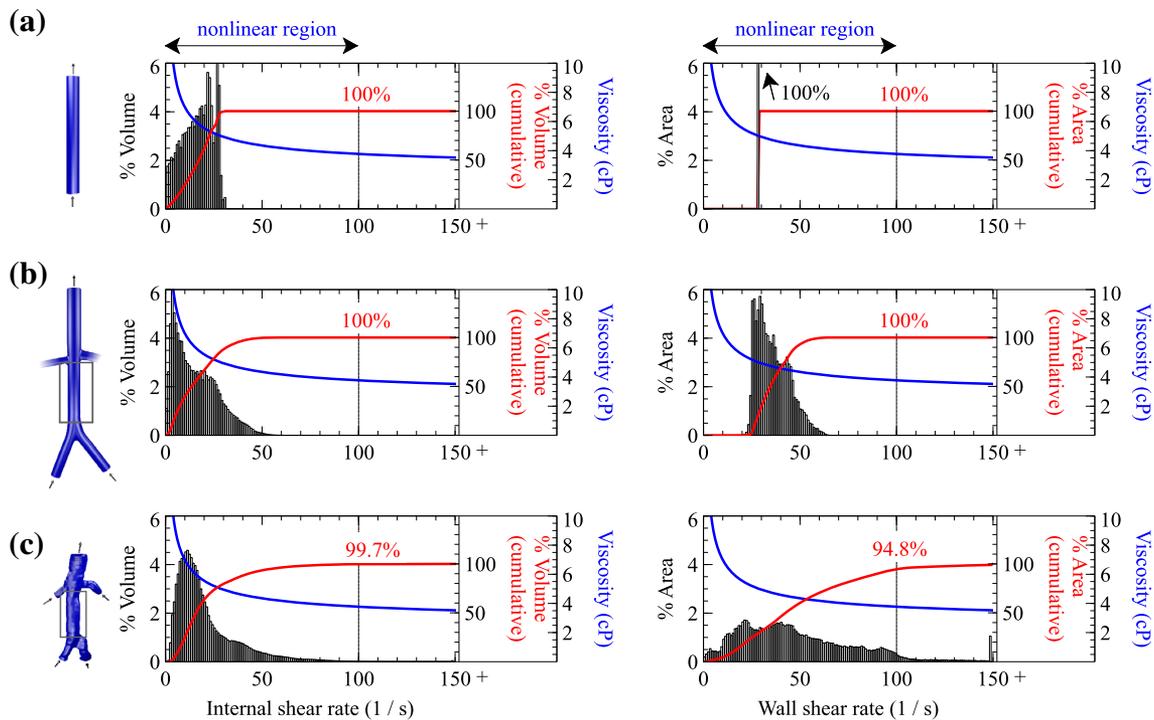


**FIGURE 3.** Internal and wall shear rate histograms from the non-Newtonian simulation results (bars), non-Newtonian shear rate–viscosity curve for blood (blue), and cumulative shear rate (red) for the (a) straight tube, (b) patient-averaged, and (c) scaled patient-specific IVCs. The cumulative shear rates annotated at the location  $\dot{\gamma} = 100\text{s}^{-1}$  quantify how much of the IVC volume or wall surface area lies in the nonlinear region of the shear rate–viscosity curve for blood ( $\dot{\gamma} < 100\text{s}^{-1}$ ).

$\rho = 1060 \text{ kg m}^{-3}$ . Boundary conditions were specified as in Aycock *et al.*<sup>1</sup> Specifically, a zero-pressure Dirichlet boundary condition was specified at the outlet and the gradient of the pressure was fixed at zero at the inlets (Neumann boundary condition). Steady flow rates were specified at the inlets, consistent with *in vivo* magnetic resonance imaging measurements of normal resting flow in the IVC:<sup>9</sup> 0.6 LPM inflow for each iliac vein and 0.4 LPM inflow for each renal vein.<sup>9</sup> For the straight-tube IVC, a steady flow rate of 1.2 LPM was specified at the inlet, representative of the combined flow from the left and right iliac veins. Fully-developed Newtonian or non-Newtonian flow was specified at all inlets by extruding the inlets beyond their entry lengths and computing the fully developed flow that was then prescribed to each respective inlet.

The CFD results were post-processed to obtain velocity, viscosity, shear rate, and shear stress information. Thrombus wake volumes were also quantified by integrating the volume of the flow in the vicinity of the thrombus where the velocity magnitude was less than  $1 \text{ cm s}^{-1}$ , similar to the stasis or stagnation volume definitions used in previous hemodynamic studies.<sup>18,25</sup> The elapsed computational time (or “wall clock” time) required for convergence (defined as a reduction of the residuals to less than  $10^{-6}$  and  $10^{-9}$  for pressure and velocity, respectively) was recorded to compare the

computational cost of the Newtonian vs. the non-Newtonian simulations.

## RESULTS

### Unoccluded IVCs

#### Hemorheological Comparison

More than 99% of the internal shear rates in the infrarenal region of the IVCs are found to lie in the nonlinear region (i.e., less than  $100 \text{ s}^{-1}$ ) of the shear rate–viscosity curve for blood (Fig. 3). The Newtonian simulations performed using the asymptotic viscosity for blood over-predict the non-Newtonian Reynolds numbers by more than a factor of two (Table 2). The Newtonian and non-Newtonian Reynolds numbers are much closer when the characteristic viscosity is used in the Newtonian simulations (Table 2). Non-Newtonian importance factors ( $\mu_c/\mu_\infty$ ) are also higher than the threshold of 1.75 suggested by Ballyk *et al.*<sup>3</sup> for all IVCs (Table 2).

Use of a characteristic viscosity improves the prediction of velocity, viscosity, shear rate, and shear stress profiles (Fig. 4). When using the asymptotic viscosity, velocity profiles are less smooth and have an increased number of inflection points compared with the characteristic viscosity and non-Newtonian results

**TABLE 2.** Average shear rate calculated using the Poiseuille approximation ( $\dot{\gamma}_p$ ; Eq. 1), characteristic shear rate calculated using a volume-weighted average of the asymptotic Newtonian simulation results ( $\dot{\gamma}_c$ ; Eq. 2), characteristic shear rate calculated using a volume-weighted average of the non-Newtonian simulation results ( $\dot{\gamma}_{c,n-N}$ ), characteristic viscosity ( $\mu_c$ ), non-Newtonian importance factor ( $\mu_c/\mu_\infty$ ), and Reynolds numbers in the infrarenal region of the IVCs.

IVC geometry	Case	$\dot{\gamma}$ ( $s^{-1}$ )				$Re(\mu)$			
		$\dot{\gamma}_p$	$\dot{\gamma}_c$	$\dot{\gamma}_{c,n-N}$	$\mu_c$ (cP)	$\mu_c/\mu_\infty$	$\mu = \mu_{c,n-N}$	$\mu = \mu_\infty$	$\mu = \mu_c$
Straight-tube	IVC	17.0	17.0	16.4	5.85	2.28	229	525	231
	+filter		20.4	19.1	5.53	2.15	240		244
	+clot		25.9	24.0	5.15	2.00	257		262
Patient-averaged	IVC	17.8	17.1	15.8	5.84	2.27	224	522	230
	+filter		19.6	18.1	5.59	2.18	234		239
	+clot		23.7	22.2	5.28	2.05	249		254
Patient-specific	IVC	17.0	24.0	21.0	5.27	2.05	248	527	257
	+filter		26.6	23.6	5.11	1.99	255		265
	+clot		31.4	28.6	4.88	1.90	270		278

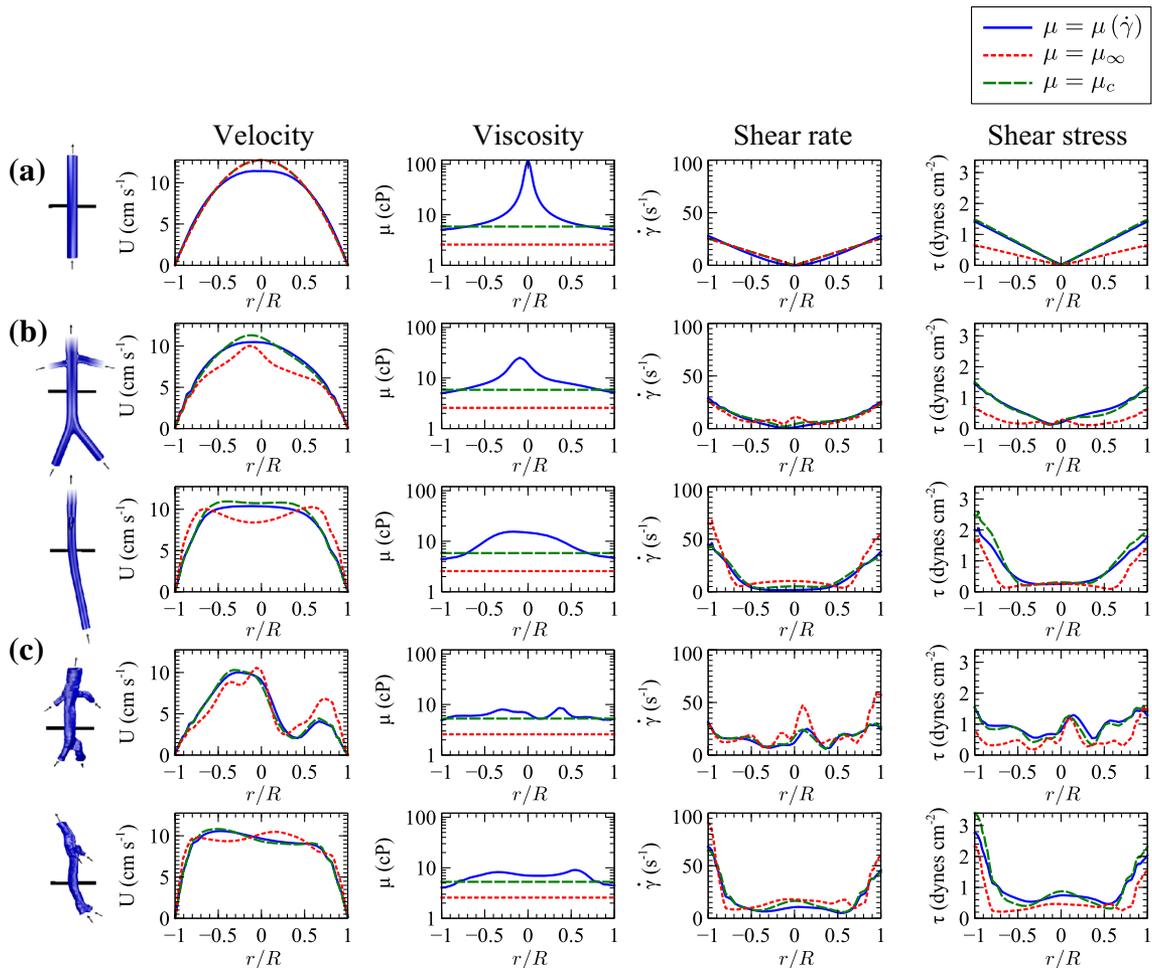


**FIGURE 4.** Velocity, viscosity, shear rate, and shear stress profiles along lines identified in the left-most images for the unoccluded (a) straight-tube, (b) patient-averaged, and (c) scaled patient-specific IVCs. The radius is normalized by the maximum radius ( $R \approx 1$  cm).

(Fig. 4). The mean non-Newtonian WSS is under-predicted when using the asymptotic viscosity (%ME of  $-29\%$  to  $-54\%$ ), and slightly over-predicted when using the characteristic viscosity (%ME of  $5\%$ – $11\%$ ; Table 3).

Secondary flows are also better predicted using the characteristic viscosity compared with the asymptotic viscosity (Figs. 5 and 6). Secondary flow velocities are larger when using the asymptotic viscosity compared with the characteristic viscosity or non-Newtonian

**TABLE 3. Average flow parameters and Newtonian approximation errors for flow through the infrarenal region of the straight-tube, patient-averaged, and scaled patient-specific IVCs unoccluded, with an IVC filter, and with an IVC filter and a thrombus.**

$\phi$ (units)	IVC geometry	Case	Non-Newtonian		Newtonian			
			$\mu = \mu(\dot{\gamma})$		$\mu = \mu_{\infty}$		$\mu = \mu_c$	
			$\bar{\phi}_{n-N}$	%SD	$\bar{\phi}_N$	%ME	$\bar{\phi}_N$	%ME
$\mu_{\text{wall}}$ (cP)	Straight-tube	IVC	5.02	–			5.85	16
		+ filter	4.89	14	2.57	–48	5.52	13
		+ thrombus	4.71	11			5.15	9
	Patient-averaged	IVC	4.76	6				
		+ filter	4.67	10	2.57	–45	5.59	20
		+ thrombus	4.53	10			5.28	17
	Patient-specific	IVC	4.87	34				
		+ filter	4.79	37	2.57	–46	5.11	7
		+ thrombus	4.72	55			4.89	3
$WSR$ ( $s^{-1}$ )	Straight-tube	IVC	28.3	–			25.5	–10
		+ filter	33.4	24	31.1	–7	31.2	–7
		+ thrombus	43.7	65	40.9	–6	40.8	–7
	Patient-averaged	IVC	36.2	23	43.0	19	32.3	–11
		+ filter	39.7	25	46.7	18	36.4	–8
		+ thrombus	49.1	58	55.2	12	45.4	–8
	Patient-specific	IVC	48.7	65	58.1	19	43.6	–11
		+ filter	52.6	63	62.5	19	48.2	–8
		+ thrombus	62.6	69	70.8	13	57.7	–8
$WSS$ ( $\text{dyn cm}^{-2}$ )	Straight-tube	IVC	1.42	–	0.66	–54	1.49	5
		+ filter	1.60	18	0.80	–50	1.72	8
		+ thrombus	1.93	47	1.05	–46	2.10	9
	Patient-averaged	IVC	1.70	17	1.10	–35	1.88	11
		+ filter	1.82	19	1.20	–34	2.03	12
		+ thrombus	2.12	43	1.42	–33	2.39	13
	Patient-specific	IVC	2.09	50	1.49	–29	2.30	10
		+ filter	2.22	49	1.61	–28	2.46	11
		+ thrombus	2.53	55	1.82	–28	2.82	12

model (Fig. 5c). Additionally, the asymptotic Newtonian viscosity simulations reveal regions of swirling flow (e.g., Fig. 6a) and different streamline trajectories than those predicted by the characteristic Newtonian viscosity or non-Newtonian simulations (e.g., Figs. 6b, 6c).

#### Effect of IVC Morphology on Hemodynamics

The range of observed internal and wall shear rates is smallest in the straight-tube IVC (Fig. 3a), larger in the patient-averaged IVC (Fig. 3b), and largest in the patient-specific IVC (Fig. 3c; see also %SD in Table 3). Mean WSR and WSS also increase with increasing morphological complexity of the IVC (Table 3).

Mean shear rates calculated using the Poiseuille flow assumption (Eq. 1) are approximately  $17 s^{-1}$  for each infrarenal IVC (Table 2). However, using the cell-volume weighted approach proposed in this study (Eq. 2), the mean shear rate is approximately 40% higher in the patient-specific IVC ( $24 s^{-1}$ ) than in the straight-tube or patient-averaged IVCs ( $17.0$  and  $17.1 s^{-1}$ , respectively; Table 2). Thus, the

characteristic viscosity is approximately 10% lower in the patient-specific IVC (Table 2). Furthermore, the non-Newtonian importance factor decreases slightly with increasing geometric complexity (Table 2) due to the attendant increase in the average shear rate.

Using the characteristic viscosity, WSS errors are approximately the same for all IVC geometries (%ME of 5–11%; Table 3). When using the asymptotic viscosity, WSS errors are larger than when using the characteristic viscosity, but decrease in magnitude with increasing geometric complexity (from a %ME of –54 to –29%; Table 3).

Increasing geometric complexity of the IVC is also associated with an increase in secondary flow velocities (Dean numbers from the non-Newtonian simulations are 0, 27, and 75 for the straight-tube, patient-averaged, and patient specific IVCs, respectively; see Figs. 5a vs. 5b). Dean vortices are symmetric in the patient-averaged IVC (Fig. 5a), but are stronger (i.e., higher secondary flow velocities) in the anatomical left side of the patient-specific IVC (Fig. 5b).

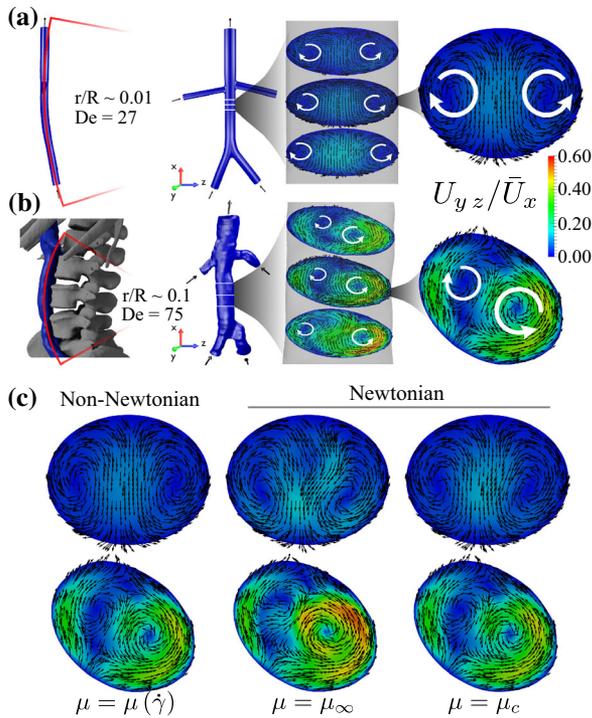


**FIGURE 5.** Secondary flow in the (a) patient-averaged and (b) scaled patient-specific IVC geometries. (c) Enlarged view of the middle cross-sections from (a) and (b) showing the effect of the viscosity model on the secondary flow patterns.

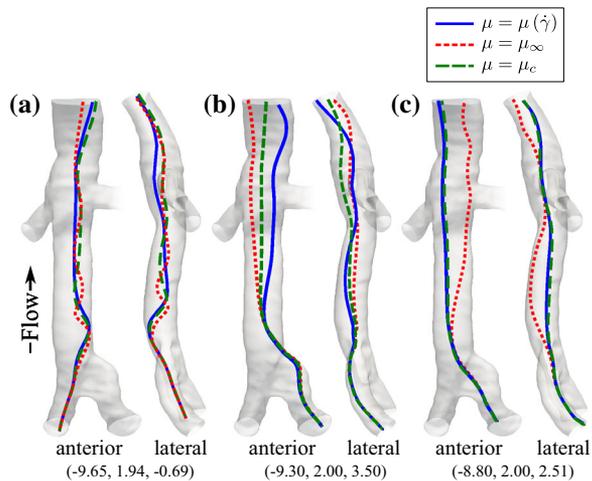


**FIGURE 6.** Streamlines in the scaled patient-specific IVC for the three viscosity models considered. The streamlines are seeded from three different locations ( $x,y,z$  coordinates, in cm) in the (a) anatomical right and (b,c) anatomical left iliac veins.

### Partially Occluded IVCs

#### Hemorheological Comparison

Partial occlusion of the IVC increases the characteristic shear rate (making it higher than the average shear rate predicted by the Poiseuille approximation;

Table 2), thus decreasing the characteristic viscosity and increasing the Reynolds number slightly (Table 2). The non-Newtonian importance factors also decrease slightly with increasing occlusion (Table 2), but are still above the threshold of 1.75 specified by Ballyk *et al.*<sup>3</sup>

As in the unoccluded IVC, mean IVC WSS is again predicted more accurately using the characteristic viscosity than using the asymptotic viscosity (%ME of 8–13% vs. %ME of –28% to –50%, respectively; Table 3). Mean WSR and WSS increase with partial occlusion of the IVC by the IVC filter, and further increase with partial occlusion of the IVC by the thrombus (Table 3). As the mean WSR and WSS increase, the mean error in WSS decreases slightly using the asymptotic viscosity, but increases slightly using the characteristic viscosity (Table 3).

Thrombus WSR values reach well over  $100 \text{ s}^{-1}$  in the region of maximum occlusion ( $x = -23 \text{ mm}$  to  $-20 \text{ mm}$ ; Figs. 7a\*–7c\*). In contrast to the previous results, in the region of maximum occlusion, the non-Newtonian WSS on the thrombus is predicted more closely using the asymptotic viscosity than using the characteristic viscosity (Figs. 7a\*–7c\*) due to the higher thrombus WSR and lower viscosity in this region. In general, the mean thrombus WSS is under-predicted relative to the non-Newtonian results when using the asymptotic viscosity (by as much as 80%) and over-predicted when using the characteristic viscosity (by as much as 50%; Fig. 7a).

The non-Newtonian thrombus wake volumes range from 13% to 15% of the thrombus volume (Table 4) and are predicted more accurately using the characteristic viscosity than using the asymptotic viscosity in the Newtonian simulations (Table 4; Fig. 8).

#### Effect of IVC Morphology on Hemodynamics

The trends noted for the unoccluded IVCs are present again in the partially occluded IVCs: mean IVC WSR and WSS increase with increasing morphological complexity of the IVC, and IVC WSS errors decrease with increasing morphological complexity of the IVC when using the asymptotic viscosity (although the WSS errors are still much larger when using the asymptotic viscosity compared with the characteristic viscosity; Table 3). However, the peak thrombus WSR and thrombus WSS decrease with increasing geometric complexity of the IVCs (Figs. 7a\*–7c\*).

Additionally, while the flow is approximately symmetric in the straight tube and patient-averaged IVCs (Figs. 8a–8b), the flow around the model thrombus is biased toward the anterior side in the scaled patient-specific IVC (Fig. 8c).

**TABLE 4. Wake volumes normalized by the thrombus volume (1.06 cm<sup>3</sup>) for the Newtonian and non-Newtonian simulations in the IVCs partially occluded by the filter and thrombus.**

IVC geometry	Non-Newtonian	Newtonian	
	$\mu = \mu(\dot{\gamma})$	$\mu = \mu_{\infty}$	$\mu = \mu_c$
Straight-tube	0.15	0.20	0.15
Patient-averaged	0.14	0.17	0.13
Patient-specific	0.13	0.15	0.13

*Computational Cost of Newtonian vs. Non-Newtonian Simulations*

Using the same number of CPUs (96) for all simulations, elapsed computational times are lowest using the characteristic viscosity, higher using the asymptotic viscosity, and highest using the non-Newtonian viscosity model (Table 5). At most, the non-Newtonian simulations require approximately 24% more computational time than the individual Newtonian simulations (Table 5). Compared to the sum of the

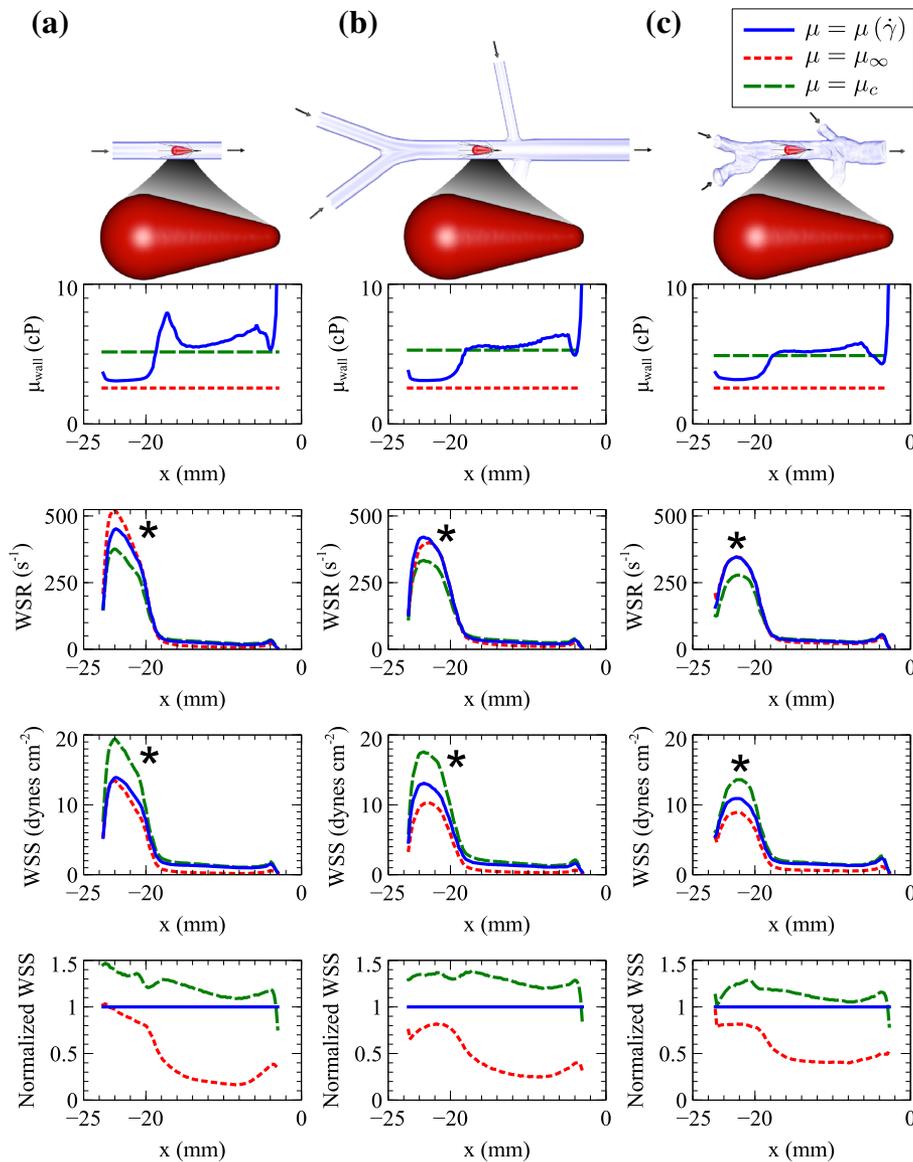


**FIGURE 7. Distribution of the circumferential averages of thrombus wall viscosity, thrombus WSR, thrombus WSS, and normalized thrombus WSS vs. axial position ( $x$ ) along the thrombus in the (a) straight-tube, (b) patient-averaged, and (c) scaled patient-specific IVCs. The location  $x = 0$  mm is approximately 2 cm upstream of where the renal veins meet the IVC and corresponds to the bottom surface of the IVC filter hub.**

computational time for the asymptotic and characteristic Newtonian simulations required in the two-step process for obtaining an improved characteristic viscosity (see “Characteristic Shear Rate and Viscosity”), the non-Newtonian simulations require approximately 50% less time (Table 5).

## DISCUSSION

In contrast to a previous study on IVC hemodynamics,<sup>45</sup> we found that non-Newtonian effects are strong in the IVC: mean errors in WSS in the infra-

renal region of the IVC are approximately  $-50$  to  $-30\%$  when using the asymptotic viscosity for blood whereas Swaminathan *et al.*<sup>45</sup> reported errors in WSS to be less than 10% using the same asymptotic viscosity. This discrepancy may be due to the higher flow rate and Reynolds number investigated in the previous study (approximately 2.31 LPM and 1000 in Swaminathan *et al.*<sup>45</sup> vs. 1.2 LPM and 225–250 here, respectively). Additionally, in the current study, over 99% of the internal shear rates in the infrarenal IVC are less than  $100 \text{ s}^{-1}$  (Fig. 3), non-Newtonian importance factors are above the threshold suggested by Ballyk *et al.*<sup>3</sup> of 1.75 (Table 2), and secondary flows are sensitive to the viscosity model (Figs. 5 and 6), collectively indicating that non-Newtonian effects are important during resting flow conditions in the IVC.

Previous studies of pulsatile blood flow have also suggested that non-Newtonian effects are generally negligible in large blood vessels like the IVC.<sup>3,26,30</sup> The discrepancy between those studies and the results reported herein may be explained by the differences in shear rates, which are well over  $100 \text{ s}^{-1}$  in most large blood vessels during systole (Fig. 1) but much less than  $100 \text{ s}^{-1}$  in the IVC (an average of approximately 17 to  $24 \text{ s}^{-1}$  based on our analysis; Table 2). Previous studies have shown that non-Newtonian effects can be significant in large arteries,<sup>3,26,30</sup> but the effects are isolated to the diastolic phase of the cardiac cycle, when the shear rates are low. Furthermore, Ballyk *et al.*<sup>3</sup> reported that non-Newtonian effects are more significant when simulating steady flow than when simulating a pulsatile flow with the same mean flow rate. Because of the damping effect of vascular compliance and the associated relatively steady flow rate in the IVC (Fig. 1c), the shear rates in the IVC are comparable to the shear rates observed in arteries during diastole. Thus, while non-Newtonian effects may be neglected in most arterial flows, where the high stresses that occur during systole are of primary interest (e.g., for predicting atherosclerosis), non-Newtonian effects are significant in the IVC throughout the entire cardiac cycle.

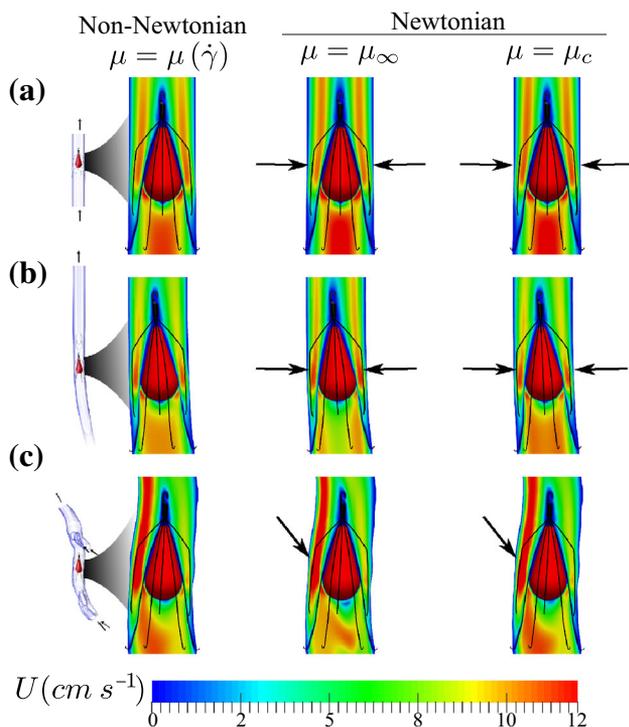


**FIGURE 8.** Contours of velocity magnitude on a sagittal plane in the IVCs partially occluded by an IVC filter and thrombus. The flow is approximately symmetric in (a) the straight-tube and (b) the patient-averaged IVCs, but the flow velocity is higher along the anterior side of (c) the scaled patient-specific IVC (arrows).

**TABLE 5.** Elapsed computational times (or wall clock times) in hours using 96 CPUs for the Newtonian ( $t_N$ ) and non-Newtonian ( $t_{n-N}$ ) simulations performed using the scaled patient-specific IVC geometry.

Case	Computational time (h)				
	Non-Newtonian $\mu = \mu(\dot{\gamma})$	Newtonian		$\max(t_{n-N}/t_N)$	$t_{n-N}/\sum t_N$
		$\mu = \mu_\infty$	$\mu = \mu_c$		
IVC	2.47	2.47	1.99	1.24	0.55
+filter	1.94	2.10	1.69	1.15	0.51
+clot	2.12	2.07	1.76	1.20	0.55

The reported values are the means of five simulations (maximum standard deviation of 0.04 h).

As shown in previous studies,<sup>2,8,21,30</sup> the use of a characteristic viscosity improves the accuracy of the Newtonian approximation for predicting the non-Newtonian WSS (%ME of 5–13%) and Reynolds numbers (Table 2) compared with the use of the asymptotic viscosity. Because the characteristic viscosities in the current study are much higher than the Newtonian viscosities used in previous studies (5.27–5.85 cP here vs. 2.57–4 cP<sup>38,39,43,50</sup>), the Reynolds numbers in the current study are the lowest reported for resting flow in the infrarenal IVC (approximately 225–250 here vs. 320–370 in the literature<sup>38,39,43,50</sup>). Consequently, the previously published studies contain greater flow disturbances (e.g., wakes) due to the IVC filter and are probably more representative of the hemodynamics that occur in the IVC under elevated flow conditions (e.g., light exercise).

However, when considering partial occlusion of the IVC, local errors in thrombus WSS are large in the high-shear region of maximum IVC occlusion (up to approximately 50%; Figs. 7a\*–7c\*) even when using a characteristic viscosity in the Newtonian simulations. The thrombus WSS errors are lower when using the asymptotic viscosity in the high-shear regions (Figs. 7a\*–7c\*). But, as the shear rate decreases downstream of the site of maximum thrombus diameter, the thrombus WSS is again predicted more accurately using the characteristic viscosity (Fig. 7). Additionally, the volume of the low-shear wake region downstream of the thrombus is predicted more accurately using the characteristic viscosity (Table 4). Indeed, when considering partial occlusion of the IVC, a single viscosity cannot simultaneously predict the flow in the region of the occlusion, where shear rates are high and the viscosity is relatively low (Figs. 7a\*–7c\*), and in the regions upstream and downstream of the occlusion, where the shear rates are low and the viscosity is relatively high (Fig. 7). Thus, use of a non-Newtonian model is preferable if accurate predictions of thrombus WSS are required—e.g., for predicting thrombolysis, thrombosis, and embolization,<sup>4</sup> all of which are mediated by fluid stresses either directly (e.g., mechanical lysis<sup>43</sup>), indirectly (e.g., platelet activation leading to thrombus growth<sup>34</sup>), or both.

The added computational cost of using a non-Newtonian model was found to be relatively low (at most 24% more expensive; Table 5). Furthermore, the computational cost of performing a single non-Newtonian simulation is approximately 50% of the time required to perform two Newtonian simulations to better approximate the non-Newtonian characteristic viscosity (Table 5) using the approach presented herein. Other recent studies<sup>29,32,48</sup> have also shown that non-Newtonian simulations can be performed with approximately the same computational cost as New-

tonian simulations, or even less. Collectively, these results challenge the notion (e.g., see discussion in Benard *et al.*,<sup>5</sup> Mejia *et al.*,<sup>33</sup> Vahidi and Fatouraei,<sup>49</sup> and Marrero *et al.*<sup>32</sup>) that added computational cost is a strong justification for neglecting non-Newtonian effects.

The inherent simplicity (e.g., Surovtsova<sup>44</sup>) and stability (e.g., Vahidi and Fatouraei<sup>49</sup>) of the Newtonian model are also sometimes provided as justification for neglecting non-Newtonian effects, but we found that the non-Newtonian Carreau model was no more challenging to use and was just as numerically stable as the Newtonian model. Thus, the strongest justification for neglecting non-Newtonian effects in CFD simulations of blood flow is the prevalence of high shear rates (e.g., Torii *et al.*<sup>47</sup> and Clark *et al.*<sup>14</sup>) in the flow field of interest. However, even then, one must ensure that regions of low shear rate are not simultaneously present, where non-Newtonian effects could affect the solution.

In addition to hemorrheology, our results show that IVC morphology has a strong influence on IVC hemodynamics. Specifically, as IVC complexity increases, the range of shear rates present in the IVC also increases (Fig. 3) and the flow patterns in the IVC become increasingly complex (Fig. 4). Furthermore, in the patient-averaged and patient-specific IVCs, Dean vortices develop in the infrarenal IVC due to the curvature of the IVC along the lumbar spine (Fig. 5), introducing swirl into the flow and altering the fluid streamlines (e.g., Fig. 6). We suspect that, as shown in a recent study on arterial emboli,<sup>35</sup> patient-specific secondary flow features may affect the trajectory of migrating emboli in the IVC and possibly influence the embolus-trapping efficiency of IVC filters.

Some limitations should be noted. Only one non-Newtonian model (Carreau) and one set of model constants were considered. Furthermore, the asymptotic viscosity of blood is approximately 3.5 cP for a nominal hematocrit of 45%,<sup>12,37</sup> while a value of 2.57 cP was used in the current study, which was based on the curve fit of Swaminathan *et al.*<sup>45</sup> to the experimental data of Chien.<sup>11</sup> Blood viscosity and shear-thinning behavior are patient-specific and increase with increasing blood hematocrit;<sup>12</sup> therefore, a wide range of model constants should be studied. However, the purpose of this study was to investigate representative physiological conditions, and to determine if, in general, non-Newtonian effects are important in the human IVC. We chose to use the same model and model constants as those in Swaminathan *et al.*<sup>45</sup> to permit a direct comparison with that study, which is often cited as justification for neglecting non-Newtonian effects in the human IVC. We expect that the use of different model constants and a higher asymptotic

viscosity (e.g., 3.5 cP) would affect the quantitative comparison of the Newtonian and non-Newtonian results, but would not change the overall results and conclusions of this study, namely that non-Newtonian effects are significant in the human IVC and should be considered in future studies of IVC hemodynamics.

Additionally, IVC hemodynamics were investigated in only one patient-specific IVC using an idealized thrombus model and average boundary conditions rather than patient-specific measurements. Other patient geometries would have different levels of infrarenal curvature, iliac vein compression,<sup>36</sup> and cross-sectional variation. However, the patient-specific IVC in the current study is representative of a normal, healthy patient. Furthermore, the results of this study demonstrate that subtle differences in IVC morphology can influence IVC filter placement mechanics (e.g., contact forces; Table 1) and IVC hemodynamics (e.g., secondary flow; Figs. 5 and 6), thus motivating the need for further investigation of the influence of patient-specific IVC morphology on IVC filter performance. These results also motivate future fluid-structure interaction studies to quantify the effect of wall motion on IVC mechanics and hemodynamics. Finally, although beyond the scope of the present study, validation studies should be performed in future work to compare results from the computational model to results from *in vitro* models and, eventually, to state-of-the-art *in vivo* measurements of IVC mechanics and hemodynamics.

## SUMMARY

- (1) Shear rates are low in the IVC geometries considered, with over 99% of the infrarenal IVC volume in the highly nonlinear region of the shear rate–viscosity curve. Furthermore, non-Newtonian importance factors are above the threshold specified by Ballyk *et al.*<sup>3</sup> in all cases, indicating that non-Newtonian effects are important in the IVC.
- (2) The Newtonian simulations performed using an asymptotic viscosity greatly under-predict the non-Newtonian WSS (%ME of -28% to -54%). Simulations performed using the characteristic viscosity predict the non-Newtonian WSS more closely (%ME of 5–13%), but cannot accurately model the hemodynamics for the full range of shear rates that occur, especially in the presence of the high shear rates generated during partial occlusion of the IVC.

- (3) Non-Newtonian simulations required only a marginal increase in computational time (15–24% longer wall clock time) compared with the Newtonian simulations. Therefore, we recommend that future studies of blood flow in the IVC consider non-Newtonian effects, especially when accurate predictions of both low ( $<100\text{ s}^{-1}$ ) and high ( $>100\text{ s}^{-1}$ ) shear rate phenomenon are required.
- (4) Infrarenal IVC flow patterns become increasingly complex with increasing anatomical complexity of the IVC. Secondary flow features are also sensitive to the viscosity model and are more prominent in the Newtonian simulations performed using the asymptotic viscosity due to the associated higher Reynolds number. We anticipate that these secondary flow patterns may influence embolus trajectories and IVC filter embolus-trapping efficiencies. Thus, future studies should also recognize the potential limitations of using an idealized IVC model to predict IVC filter performance.

## ACKNOWLEDGMENTS

The authors thank Elaheh Rahbar, Daisuke Mori, and James E. Moore Jr. for generously providing the geometry for the patient-averaged IVC model. This research was supported by the Walker Assistantship program at the Penn State Applied Research Laboratory.

## REFERENCES

- <sup>1</sup>Aycock, K. I., R. L. Campbell, K. B. Manning, S. P. Sastry, S. M. Shontz, F. C. Lynch, and B. A. Craven. A computational method for predicting inferior vena cava filter performance on a patient-specific basis. *J. Biomech. Eng.* 136:1–13, 2014. Erratum, 137:1–2, 2015.
- <sup>2</sup>Baaijens, J. P. W. Numerical analysis of steady generalized Newtonian blood flow in a 2D model of the carotid artery bifurcation. *Biorheology* 30:63–74, 1993.
- <sup>3</sup>Ballyk, P. D., D. A. Steinman, and C. R. Ethier. Simulation of non-Newtonian blood flow in an end-to-side anastomosis. *Biorheology* 31:565–86, 1994.
- <sup>4</sup>Basmadjian, D. Embolization: critical thrombus height, shear rates, and pulsatility. patency of blood vessels. *J. Biomed. Mater. Res.* 23:1315–1326, 1989.
- <sup>5</sup>Benard, N., R. Perrault, and D. Coisne. Computational approach to estimating the effects of blood properties on changes in intra-stent flow. *Ann. Biomed. Eng.* 34:1259–1271, 2006.

- <sup>6</sup>Bird, R. B., R. C. Armstrong, and O. Hassager. Dynamics of polymeric liquids. Vol. 1, Fluid mechanics, New York: Wiley, 1987.
- <sup>7</sup>Chaikof, E. L., M. F. Fillinger, J. S. Matsumura, R. B. Rutherford, G. H. White, J. D. Blankensteijn, V. M. Bernhard, P. L. Harris, K. C. Kent, J. May, F. J. Veith, and C. K. Zarins. Identifying and grading factors that modify the outcome of endovascular aortic aneurysm repair. *J. Vasc. Surg.* 35:1061–1066, 2002.
- <sup>8</sup>Chen, J., X.-Y. Lu, and W. Wang. Non-Newtonian effects of blood flow on hemodynamics in distal vascular graft anastomoses. *J. Biomech.* 39:1983–95, 2006.
- <sup>9</sup>Cheng, C. P., R. J. Herfkens, and C. A. Taylor. Inferior vena caval hemodynamics quantified in vivo at rest and during cycling exercise using magnetic resonance imaging. *Am. J. Physiol. Heart Circ. Physiol.* 284:H1161–7, 2003.
- <sup>10</sup>Cherry, E. M. and J. K. Eaton. Shear thinning effects on blood flow in straight and curved tubes. *Phys. Fluids* 25:073104, 2013.
- <sup>11</sup>Chien, S. Shear dependence of effective cell volume as a determinant of blood viscosity. *Science* 168:977–979, 1970.
- <sup>12</sup>Cho, Y. I. and K. R. Kensey. Effects of the non-Newtonian viscosity of blood on flows in a diseased arterial vessel. part 1: steady flows. *Biorheology* 28:241–62, 1991.
- <sup>13</sup>Cipolla, J., N. S. Weger, R. Sharma, S. P. Schrag, B. Sarani, M. Truitt, M. Lorenzo, C. A. Sims, P. K. Kim, D. Torigian, B. Temple-Lykens, C. P. Sicoutris, and S. P. Stawicki. Complications of vena cava filters: a comprehensive clinical review. *OPUS 12 Scientist* 2:11–24, 2008.
- <sup>14</sup>Clark, W. D., B. A. Eslahpazir, I. R. Argueta-Morales, A. J. Kassab, E. A. Divo, and W. M. DeCampi. Comparison between bench-top and computational modelling of cerebral thromboembolism in ventricular assist device circulation. *Cardiovasc. Eng. Technol.* 6:242–255, 2015.
- <sup>15</sup>Couch, G. G., H. Kim, and M. Ojha. In vitro assessment of the hemodynamic effects of a partial occlusion in a vena cava filter. *J. Vasc. Surg.* 25:663–72, 1997.
- <sup>16</sup>Dowell, J. D., J. C. Castle, M. Schickel, U. K. Andersson, R. Zielinski, E. McLoney, G. Guy, X. Yang, and S. Ghadiali. Celest inferior vena cava wall strut perforation begets additional strut perforation. *J. Vasc. Interv. Radiol.* 26:1510–1518.e3, 2015.
- <sup>17</sup>Fortuny, G., J. Herrero, D. Puigjaner, C. Olivé, F. Marimon, J. Garcia-Bennett, and D. Rodríguez. Effect of anti-coagulant treatment in deep vein thrombosis: a patient-specific computational fluid dynamics study. *J. Biomech.* 48:2047–2053, 2015.
- <sup>18</sup>Fraser, K. H. and T. Zhang. Computational fluid dynamics analysis of thrombosis potential in left ventricular assist device drainage cannulae. *ASAIO J.* 56:157–163, 2010.
- <sup>19</sup>García, A., S. Lerga, E. Peña, M. Malve, A. Laborda, M. A. De Gregorio, and M. A. Martínez. Evaluation of migration forces of a retrievable filter: experimental setup and finite element study. *Med. Eng. Phys.* 34:1167–1176, 2012.
- <sup>20</sup>Gasser, T. C., R. W. Ogden, and G. A. Holzapfel. Hyperelastic modelling of arterial layers with distributed collagen fibre orientations. *J. R. Soc. Interface* 3:15–35, 2006.
- <sup>21</sup>Gijssen, F. J., E. Allanic, F. N. van de Vosse, and J. D. Janssen. The influence of the non-Newtonian properties of blood on the flow in large arteries: unsteady flow in a 90° curved tube. *J. Biomech.* 32:705–13, 1999.
- <sup>22</sup>Goldsmith, H. and V. Turitto. Rheological aspects of thrombosis and haemostasis: basic principles and applications. *Thromb. Haemost.* 55:415–35, 1986.
- <sup>23</sup>Grassi, J. Inferior vena cava filters: analysis of five currently available devices. *Am. J. Roentgenol.* 156:813–21, 1991.
- <sup>24</sup>Hernández, Q. and E. Peña. Failure properties of vena cava tissue due to deep penetration during filter insertion. *Biomech. Model Mechanobiol.* 2015. doi:10.1007/s10237-015-0728-3.
- <sup>25</sup>Itatani, K., K. Miyaji, T. Tomoyasu, Y. Nakahata, K. Ohara, S. Takamoto, and M. Ishii. Optimal conduit size of the extracardiac fontan operation based on energy loss and flow stagnation. *Ann. Thorac. Surg.* 88:565–72; discussion 572–3, 2009.
- <sup>26</sup>Johnston, B. M., P. R. Johnston, S. Corney, and D. Kilpatrick. Non-Newtonian blood flow in human right coronary arteries: transient simulations. *J. Biomech.* 39:1116–28, 2006.
- <sup>27</sup>Kundu, P. K. and I. M. Cohen. Fluid mechanics, San Diego: Academic Press, 2008.
- <sup>28</sup>Kuy, S. R., A. Dua, C. J. Lee, B. Patel, S. S. Desai, A. Dua, A. Szabo, and P. J. Patel. National trends in utilization of inferior vena cava filters in the united states, 2000–2009. *J. Vasc. Surg. Venous Lymphat. Disord.* 2:15–20, 2014.
- <sup>29</sup>Kwack, J. A. and A. Masud. A stabilized mixed finite element method for shear-rate dependent non-Newtonian fluids: 3D benchmark problems and application to blood flow in bifurcating arteries. *Comput. Mech.* 53(4):751–776 2013.
- <sup>30</sup>Lee, S.-W. and D. A. Steinman. On the relative importance of rheology for image-based CFD models of the carotid bifurcation. *J. Biomech. Eng.* 129:273–278, 2007.
- <sup>31</sup>Mann, D. E. and J. M. Tarbell. Flow of non-Newtonian blood analog fluids in rigid curved and straight artery models. *Biorheology* 27:711–733, 1990.
- <sup>32</sup>Marrero, V. L., J. A. Tichy, O. Sahni, and K. E. Jansen. Numerical study of purely viscous non-Newtonian flow in an abdominal aortic aneurysm. *J. Biomech. Eng.* 136:1–10, 2014.
- <sup>33</sup>Mejia, J., R. Mongrain, and O. F. Bertrand. Accurate prediction of wall shear stress in a stented artery: Newtonian versus non-Newtonian models. *J. Biomech. Eng.* 133:074501, 2011.
- <sup>34</sup>Moiseyev, G. and P. Z. Bar-Yoseph. Computational modeling of thrombosis as a tool in the design and optimization of vascular implants. *J. Biomech.* 46:248–52, 2013.
- <sup>35</sup>Mukherjee, D., J. Padilla, and S. C. Shadden. Numerical investigation of fluid-particle interactions for embolic stroke. *Theor. Comput. Fluid Dyn.* 30:23–29, 2016.
- <sup>36</sup>Oguzkurt, L., U. Ozkan, S. Ulsan, Z. Koc, and F. Tercan. Compression of the left common iliac vein in asymptomatic subjects and patients with left iliofemoral deep vein thrombosis. *J. Vasc. Interv. Radiol.* 19:366–370, 2008.
- <sup>37</sup>Papaioannou, T. G. and C. Stefanadis. Vascular wall shear stress: basic principles and methods. *Hellenic J. Cardiol.* 46:9–15, 2005.
- <sup>38</sup>Rahbar, E., D. Mori, and J. E. Moore. Three-dimensional analysis of flow disturbances caused by clots in inferior vena cava filters. *J. Vasc. Interv. Radiol.* 22:835–42, 2011.
- <sup>39</sup>Singer, M. A., W. D. Henshaw, and S. L. Wang. Computational modeling of blood flow in the trapease inferior vena cava filter. *J. Vasc. Interv. Radiol.* 20:799–805, 2009.

- <sup>40</sup>Singer, M. A. and S. L. Wang. Modeling blood flow in a tilted inferior vena cava filter: does tilt adversely affect hemodynamics? *J. Vasc. Interv. Radiol.* 22:229–35, 2011.
- <sup>41</sup>Smouse, B. and A. Johar. Is market growth of vena cava filters justified? *Endovasc. Today* 9:74–77, 2010.
- <sup>42</sup>Stein, P. D., F. Kayali, and R. E. Olson. Twenty-one-year trends in the use of inferior vena cava filters. *Arch. Intern. Med.* 164:1541–1545, 2004.
- <sup>43</sup>Stewart, S. F. C., R. A. Robinson, R. A. Nelson, and R. A. Malinauskas. Effects of thrombosed vena cava filters on blood flow: flow visualization and numerical modeling. *Ann. Biomed. Eng.* 36:1764–81, 2008.
- <sup>44</sup>Surovtsova, I. Effects of compliance mismatch on blood flow in an artery with endovascular prosthesis. *J. Biomech.* 38:2078–2086, 2005.
- <sup>45</sup>Swaminathan, T. N., H. H. Hu, and A. A. Patel. Numerical analysis of the hemodynamics and embolus capture of a Greenfield vena cava filter. *J. Biomech. Eng.* 128:360–70, 2006.
- <sup>46</sup>Thurston, G. B. Frequency and shear rate dependence of viscoelasticity of human blood. *Biorheology* 10:375–381, 1973.
- <sup>47</sup>Torii, R., M. Oshima, T. Kobayashi, K. Takagi, and T. E. Tezduyar. Fluid-structure interaction modeling of blood flow and cerebral aneurysm: significance of artery and aneurysm shapes. *Comput. Methods Appl. Mech. Eng.* 198:3613–3621, 2009.
- <sup>48</sup>Trias, M., A. Arbona, J. Massó, B. Miñano, and C. Bona. FDA's nozzle numerical simulation challenge: non-Newtonian fluid effects and blood damage. *PLoS One* 9:e92638, 2014.
- <sup>49</sup>Vahidi, B. and N. Fatourae. Large deforming buoyant embolus passing through a stenotic common carotid artery: a computational simulation. *J. Biomech.* 45:1312–22, 2012.
- <sup>50</sup>Wang, S. L. and M. A. Singer. Toward an optimal position for inferior vena cava filters: computational modeling of the impact of renal vein inflow with celect and trapease filters. *J. Vasc. Interv. Radiol.* 21:367–74, 2010.